Astron. Astrophys. 353, 1094–1100 (2000)

ASTRONOMY AND ASTROPHYSICS

On weak magnetic flux structures of the Sun

F. Stolpe and F. Kneer

Universitäts-Sternwarte, Geismarlandstrasse 11, 37083 Göttingen, Germany (fstolpe@uni-sw.gwdg.de)

Received 19 May 1999 / Accepted 28 July 1999

Abstract. The micro-image-scanner of the Gregory Coudé Telescope at the Observatorio del Teide/Tenerife is used for observations of structures with weak magnetic flux in the solar atmosphere. The methods for the data reduction are chosen carefully to achieve the highest possible performance, also with respect to the needs of handling large amounts of data. A lower detection limit of magnetic flux on the Sun of $2\,10^8$ Wb on an area of $0\farcs67\times0\farcs67$ was achieved.

Magnetic structures of weak magnetic flux are observed using different spectral lines in network and intra-network regions at disk center of the Sun. The present study deals mainly with a high spatial resolution observation in the magnetically sensitive Fe I 630.25 nm line. We find that weak flux may appear almost everywhere in the granular pattern, with a 65 % preference for intergranular spaces. Some elements have diameters of 2″–3″with substructure and distorted shape. Many elements are very small, $<1''$. From the ubiquitous appearance of weak magnetic flux structures in the granular pattern, in regions of both upward and downward flow, and in regions of line weakening and line enhancement, we argue that their magnetic pressure may not exceed the granular flow pressure. This gives an upper limit of the amplitude of the magnetic flux density of $|B| = 5.5\,10^{-2}$ T in agreement with the result by Keller et al. (1994)[1,2].

Key words: Sun: magnetic fields – Sun: photosphere – techniques: polarimetric

1. Introduction

Solar magnetic fields are known to show a wide range of spatial scales and magnetic flux. The rates of magnetic flux emergence (Durney et al. 1993; Petrovay & Szakály 1993) and energy release of solar structures (Withbroe & Noyes 1977) emphasize the importance of weak flux structures like intra-network (IN) magnetic elements. Table 1 shows that the daily rate of flux emergence on the whole Sun by IN elements is possibly a factor of 10^4 larger than that in active regions.

Table 1. Daily rates of magnetic flux emergence for various magnetic regions, after Durney et al. 1993 and Petrovay & Szakály 1993.

structure	rate of flux emergence
active regions	10^{12} Wb d^{-1}
ephemeral bipolar magnetic regions	10^{14} Wb d^{-1}
intra-network fields	10^{16} Wb d^{-1}

To balance the energy losses of the quiet corona a permanent energy flux of $1.8\,10^{21}$ J s^{-1} is needed. Wang et al. (1996) estimate a lower limit of $1.2\,10^{21}$ J s^{-1} for the energy release by the dissipation of IN elements. The importance of IN magnetic flux was also emphasized recently by Meunier et al. (1998) who used polarimetric observations of the infra-red Fe I lines 1.5648 μm and 1.5652 μm to estimate the intrinsic field strength of the weak flux elements and their relative contribution to the total magnetic flux.

The IN flux was discovered by Smithson (1975) and Livingston & Harvey (1975) using magnetographic techniques. From observations made with the video-magnetograph of the Big Bear Solar Observatory (BBSO) Martin (1988) and Wang (1988) determined morphological parameters of network and intra-network elements. Exploiting the ability of the BBSO video-magnetograph to take deep (long exposure) magnetograms and thus to study the temporal evolution of weak magnetic structures, Wang et al. (1995), Wang et al.(1996), Nindos & Zirin (1998), Zhang et al. (1998a, b), developed a detailed scenario of the properties of IN elements and their surrounding areas.

Keller et al. (1994) determined the intrinsic flux density of IN elements using the ZIMPOL I instrument and the line ratio method. From their analysis they derived an intrinsic flux density of definitely less than 100 mT with a probability of 68 % for less than 50 mT. Using a pair of magnetic sensitive Fe I lines in the near infrared and applying the line ratio method Lin (1995) noticed a flux tube population with a weak intrinsic flux density of ≈ 50 mT.

In addition to the IN elements, two further components of weak magnetic flux are observed on the Sun: the horizontal intra-network fields, described by Lites et al. (1996) and the

Send offprint requests to: F. Stolpe

[1] $1\,\mathrm{Wb} = 1\,\mathrm{V\,s} = 10^8\,\mathrm{Mx}$

[2] $1\,\mathrm{T} = 1\,\mathrm{V\,s\,m^{-2}} = 10^4\,\mathrm{Gauss}$

turbulent background field, investigated e.g. by Stenflo (1982) and Faurobert-Scholl (1996).

The present contribution deals with magnetic IN structures with the aim at obtaining additional knowledge about their properties. Encouraged by results by Kneer & Stolpe (1996) and Stolpe & Kneer (1997) we use an image scanning device and a Stokes-V polarimeter with short exposures. Our emphasis is on high spatial resolution, while we sacrifice on polarimetric accuracy. The following Sect. 2 describes the observations, Sect. 3 the data reduction. We present the results in Sect. 4, and Sect. 5 concludes the paper.

2. Observations

The observations discussed here were taken in June 1997 with the Gregory Coudé Telescope (GCT) at the Observatorio del Teide on Tenerife. On one day polarimetric spectrograms containing the magnetically sensitive line Fe I 630.25 nm line ($g_{\rm eff} = 2.5$) were taken, on another day the adjacent Fe I 630.15 nm line ($g_{\rm eff} = 1.67$) was included with a slightly lower spectral resolution than for the former observations. For the present study the inner parts of quiet (chromospheric) network near disk center were observed.

The micro-image-scanner (MISC, cf. Stolpe & Kneer 1998) and a Stokes-V polarimeter adapted to the size of a Thomson TH 7863 CCD chip with 384×286 pixels was used. The MISC allows us to observe a two-dimensional field of view with the Czerny-Turner high-resolution spectrograph of the GCT. The polarimeter uses a $\lambda/4$ retarder plate and a beam-splitting Savart plate. The (low) instrumental polarization of the GCT and of the MISC are compensated (Sánchez Almeida et al. 1995, Koschinsky & Kneer 1996). During the period of observation the remaining $Q/U \rightarrow V$ crosstalk was approximately 5%.

For temporal evolution studies (which will be presented in a forthcoming paper, but see Stolpe 1998) 120 scans were usually taken, spanning a time interval of about 78 min. Each scan consisted of 60 spectrograms from adjacent positions on the Sun separated by $0\farcs67$. The length of the slit of the spectropraph was limited to approximately $32''$ in order to have both $\frac{1}{2}(I+V)$ and $\frac{1}{2}(I-V)$ spectrograms on the same CCD chip without overlap. The slit width was 80 μm ($\widehat{=}0\farcs67$), the exposure time was 200 ms.

Slit-jaw images in continuum (582 nm), in Ca II K, and in Hα were monitored by means of video-CCDs. From time to time they were stored via a frame grabber. Fig. 1 shows an example of slit-jaw images. It gives an impression of the seeing conditions and of the target on the Sun. The scanned area contained only little weak chromospheric network.

For data reduction purposes, dark frame scans with the MISC and 25 flat field scans were taken. For the latter, the telescope's pointing to the Sun was continuously changed to smear the images of solar structures during exposure. And finally, for correlating and destretching the two spatially separated spectrograms of $\frac{1}{2}(I \pm V)$, a scan with an artificial pattern (stripes with low and high transmission) in front of the slit was recorded.

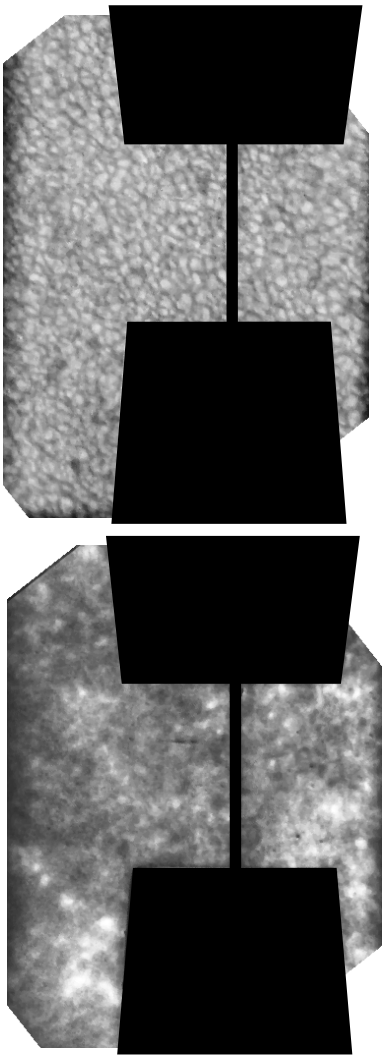

Fig. 1. Slit-jaw images taken in continuum (top), Ca II K (bottom). The length of the slit is $32''$.

3. Data reduction

We aim at detecting weak magnetic signals from the IN elements at the limit of noise. Thus the data reduction has to be done with much care. This holds also for semi-automatic treatments which are needed for the large amount of data, especially from time sequences. For each position of the scanner a separate gain table as well as the correlation of the separate $\frac{1}{2}(I \pm V)$ spectrograms for best overlap and their destretching have to be calculated and applied. For the correlation the two telluric O_2 lines contained in the spectrograms and the scan with the pattern in front of the slit are very useful. The accuracy of the physical quantities to be derived from the spectral lines is essentially limited by the accuracy of the gain tables resulting from non-exact alignments of the spectrogram pairs, i.e. from residual spectral line features in the gain tables, and from limited knowledge of the pixel sensitivities. This hampers mostly quantities taken from the Stokes-V profiles. The data reduction, then, follows the common way: Subtraction of the dark level, application of the gain

tables which removes also the effects of dust and vignetting, and subtraction of a constant level of spectrographic scattered light which was estimated by comparing the line depressions of our average spectrograms with those of the FTS-Atlas (Neckel 1987).

A noise filtering of the spectra by the "wavelet–shrinkage and thresholding" method (Donoho 1993) was applied to each line profile of each spectrum in each scan. This way of noise filtering proved to be better than a common low-pass filter.

To analyse the polarimetric signal, we decided to use the centre-of-gravity (COG) method developed by Semel (1967). It uses the wavelength distance of the $\frac{1}{2}(I+V)$ and $\frac{1}{2}(I-V)$ profiles to obtain the magnetic flux. Rees & Semel (1979) demonstrated that the COG method is independent of the pattern of the line splitting and not sensitive to the amplitude saturation of the Stokes-V signal. The accuracy is better than 10% for low line weakening (line gap effect). Del Toro Iniesta et al. (1990) mentioned that instrumental polarization and crosstalk are effects of second order on the COG method. The detection limit achieved here for the magnetic flux is $2\,10^8$ Wb on an area of $0\farcs67\times0\farcs67$, which corresponds to an average flux density of 0.8 mT.

The COG method is insensitive to the amplitude of the Stokes-V profile. Thus, comparing Stokes-V amplitudes to determine the intrinsic magnetic flux density of the IN elements proper (Stenflo 1973) is not applicable. However, Semel (1981) has shown by means of a two-component model how to use simultaneous observations of several magnetically sensitive lines to derive flux densities and area filling factors of magnetic elements. Semel's (1981) procedure was extensively applied in combination with the COG method, e.g. by del Toro Iniesta et al. (1990).

Moreover, the asymmetries of the Stokes-V amplitudes and areas are obviously not obtained with the COG method. We suggest, instead, to define the asymmetry of the intensity $y_{\rm C}$ of the COG (relative to the local continuum intensity) and of the equivalent width W by

$$\delta y_{\rm C} = \frac{y_{\rm C,blue} - y_{\rm C,red}}{y_{\rm C,blue} + y_{\rm C,red}}$$

and

$$\delta W = \frac{W_{\rm blue} - W_{\rm red}}{W_{\rm blue} + W_{\rm red}}\,,$$

respectively. δy_C and δW have similar meanings as the V amplitude- and area asymmetry, respectively. Yet, as for the amplitude- and area asymmetries, very low noise data are needed to calculate δy_C and δW. This requirement in combination with high spatial resolution has to await larger telescopes with excellent image quality. We will thus not expand further on asymmetries.

From the profiles of $\frac{1}{2}(I_\lambda \pm V_\lambda)$, treated in the above manner at each pixel in the field of view, we can compose images of quantities such as: continuum intensity, line center intensity (Stokes I), equivalent width W relative to its average, velocity $v_{\rm C}$ derived from the average of the $\frac{1}{2}(I \pm V)$ COG positions, velocity $v_{\rm min}$ from the minimum of I_λ, and the magnetic flux. Contrary to velocities derived from the zero-crossing of the V profiles, which need sufficient V signal above noise, $v_{\rm C}$ may also be measured at positions without measurable magnetic flux. The velocities $v_{\rm C}$=$v_{\rm min}$=0 are defined by the mean COG position and mean line position, respectively, in the field of view. We shall present upflow (downflow) as negative (positive) velocities.

Table 2. Statistical data derived from the selected scan. $FWHM$ means full width at half minimum intensity relative to the local continuum. The values marked with * are reference values. The lower detection limit for the magnetic flux is marked with **.

	max	min	mean	standard deviation
relative continuum intensity $I_{\rm cont}$	1.15	0.86	1.0^*	0.044
relative equivalent-width $W_{\rm rel}$	1.20	0.86	1.0^*	0.038
line center intensity $I_{\rm min}$	0.49	0.27	0.35	0.035
$FWHM$ $\Delta\lambda_{1/2}$ [pm]	12.3	9.23	10.3	0.42
velocity profile minimum $v_{\rm min}$ $[{\rm m\,s^{-1}}]$	1120	-1220	0^*	340
velocity centre-of-gravity $v_{\rm C}$ $[{\rm m\,s^{-1}}]$	1010	-1190	0^*	330
magnetic flux $\lvert\Phi\rvert$ [Wb]	$1.6\,10^9$	$2.0\,10^{8\,**}$	$3.6\,10^8$	$1.7\,10^8$

4. Results and discussion

For this first contribution of results with the MISC and its V polarimeter at the GCT we concentrate on the observation with Fe I 630.2 nm alone and select from this time sequence the scan with the highest *rms* contrast of the continuum intensity. Fig. 2, then, shows some of the two-dimensional representations of the extracted quantities. The continuum image gives an impression of the good seeing conditions and of the quality of the data, taking into account that they stem from scans and that the pixel size here is $0\farcs67\times0\farcs67$, after smoothing.

The line center intensity (image 2 in Fig. 2) has little relations, if any, with the granular intensity pattern of image 1 (cf., e.g., also Krieg et al. 1999). Close inspection shows that the brightest line center intensities occur in areas of "high" magnetic flux as is seen by comparison with the magnetogram (image 6). This is well known from line gaps in plage regions (e.g. Kneer & von Uexküll 1991 and references there). In high layers, in the chromosphere, the bright network appears, e.g. in Ca II K in areas of strong magnetic fields (see Soltau 1997 for recent references).

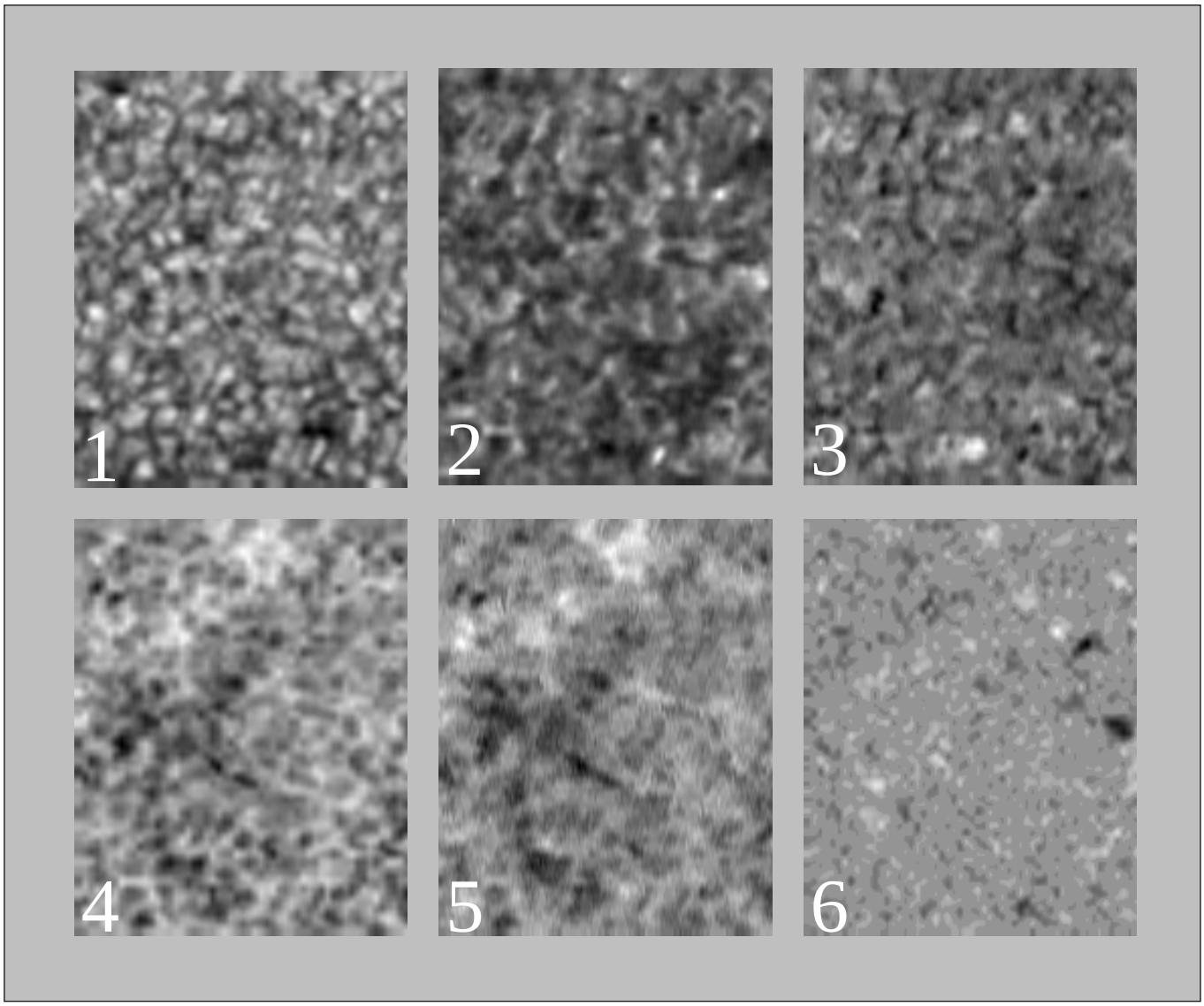

Fig. 2. Two-dimensional representations of the physical quantities from one selected scan. 1. continuum image, 2. line center intensity, 3. equivalent width, 4. Dopplergram derived from the average COG of the $\frac{1}{2}(I \pm V)$ profiles (bright = downflow), 5. Dopplergram derived form the position of the I_λ profile minima (bright = downflow), 6. magnetogram. Field of view: $32'' \times 40''$.

The relative equivalent width (image 3) does not exhibit, at first sight, clear relations to the continuum intensity or to the magnetic flux. While we shall come back to the latter below, a closer comparison of images 1 and 3 in Fig. 2 shows that enhanced equivalent widths may occur both at bright granules (close to the upper border near its center or lower part near the right border) and at dark intergranular spaces (near left border at its center or intergranules near upper right corner).

The COG velocity $v_{\rm C}$ is measured from all parts of the line profiles which, on average, stem from deeper photospheric layers than the information for the line minimum velocity $v_{\rm min}$. Thus $v_{\rm C}$ (image 4) closely resembles the continuum image (i.e. its negative representation) due to the correlation of granular flows and intensities. $v_{\rm min}$ (image 5) is coarser, the granular overshoot is barely visible. Both the $v_{\rm C}$ and the $v_{\rm min}$ image show strong downflows at small scales (bright points in images 4 and 5). They are neither related unambiguously to areas with magnetic flux (again, we shall come back to this point below) nor to bright granules or intergranules.

The magnetogram (image 6) exhibits strong magnetic flux in some few areas which coincide with the areas of brightest line center intensities and the choromspheric network. But apart from these and beyond noise, the field of view contains many IN magnetic elements with both polarities giving the well known picture of "salt and pepper". Some of the IN elements cover an area with diameter of $2''$–$3''$. Their shape is by no means roundish, they exhibit substructure and are very distorted and stretched. Many of the elements are very small, $<1''$ in diameter.

Table 2 gives part of the results of a statistical analysis for the selected scan. All data within the field of view entered into

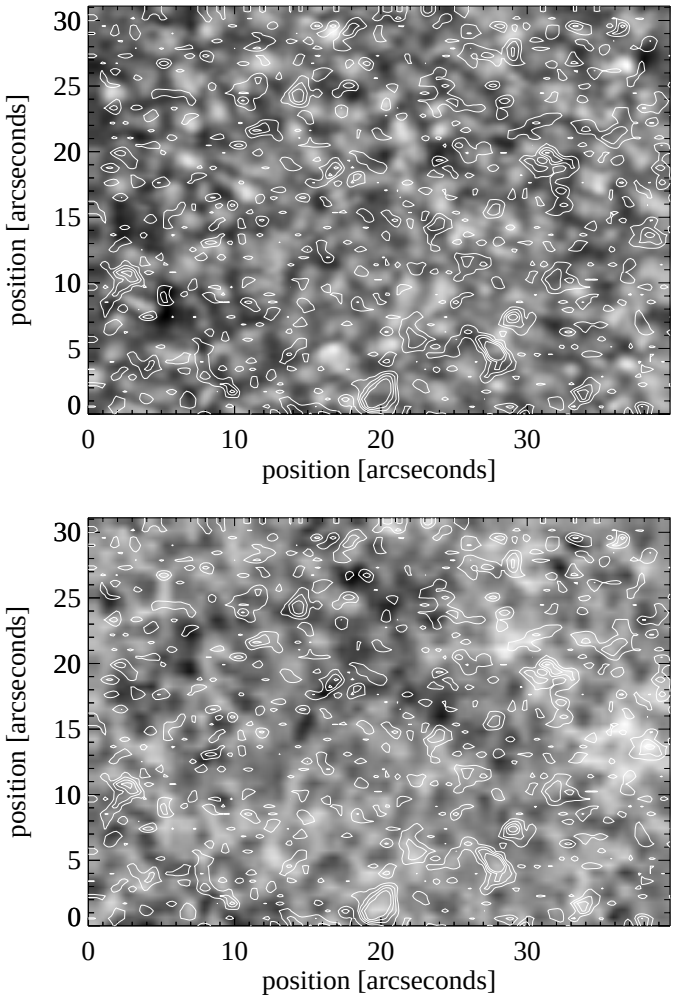

Fig. 3. Continuum image (upper) and Dopplergram $v_{\rm C}$ (lower, bright corresponding to downflow) overplotted by a contour map of the absolut value of the magnetic flux. The contour lines are at magnetic flux amplitudes of $3.0\,10^8$ Wb, $6.0\,10^8$ Wb, $9.0\,10^8$ Wb , and $12.0\,10^8$ Wb.

the analysis except for the lowest row. There, of course, only the pixels with $|\Phi| \geq 2.0\,10^8$ Wb, the lower detection limit, are used. The maximum magnetic flux $|\Phi| = 1.6\,10^9$ Wb stems from a chromospheric network area.

It is now interesting to search for the seat of the magnetic IN elements, i.e. whether they are located in granular or intergranular areas. We show in Fig. 3 again the images of the continuum intensity and of the COG velocity $v_{\rm C}$ with overlaid contours of the magnetic flux for $|\Phi| \geq 3.0\,10^8$ Wb. The magnetic flux structures possess a tendency to be located in intergranular spaces, yet many of the weak flux structures are also found sin bright granules. Similarly, the magnetic flux and the velocity are not well correlated. IN elements occur somwhat preferentially at locations of downflow, but magnetic structures at upflows are also present.

Fig. 4, then, gives scatter plots and histograms from the pixels in the field of view with $|\Phi| \geq 3.0\,10^8$ Wb, well above the detection limit. This threshold is exceeded by 595 pixels in the field of view. It substantiates the impression from Fig. 3. The

Table 3. Statistical results from the 595 pixels with $|\Phi| \geq 3.0\,10^8$ Wb in the field of view.

	limit	number of points with limit	mean total	mean with limit	standard deviation total	standard deviation with limit
relative continuum intensity $I_{\rm cont}$	≤ 1.0	386 $\hat{=}64.9\%$	0.99	0.96	0.04	0.02
Doppler velocity $v_{\rm C}[{\rm m\,s^{-1}}]$	≥ 0.0	387 $\hat{=}65.0\%$	120	320	350	220
relative equivalent width	≤ 1.0	341 $\hat{=}57.3\%$	0.99	0.97	0.04	0.02

larger part of the IN elements is located at areas with relative continuum intensity ≤ 1.0. Weak flux IN elements at areas with $I_{\rm cont,rel} > 1.0$ do also exist, though. But the corresponding histogram is definitely centered at $I_{\rm cont,rel} < 1.0$. There exists a trend for lower intensities with increasing magnetic flux amplitude.

With regard to the COG velocity $v_{\rm C}$, the low magnetic flux structures do not show a preferred sign of velocity. The structures with higher flux tend to be located at downflow areas, i.e. essentially in intergranular spaces, which is known from magnetic elements in the network and in plages. Similarly, neither the relative equivalent widths (bottom of Fig. 4) nor the line center intensities (not shown) at pixels with weak flux elements exhibit special values. Medium and "strong" flux elements tend to have reduced equivalent widths known from magnetic line gap structures. The histogram of the relative equivalent widths is centered about a value definitely < 1.0. Yet again, the very weak flux structures do not exhibit a preference for a relative equivalent width smaller or larger than 1.0.

Table 3 summarizes the statistical analysis of the pixels with $|\Phi| \geq 3.0\,10^8$ Wb. The column with the heading 'limit' gives the range from which the data are taken when the limit is set. It is seen that almost 2/3 of the selected pixels have continuum intensities ≤ 1.0. A similar percentage has downflows ($v_{\rm c} \geq 0$), while relative equivalent widths $W_{\rm rel} \leq 1.0$ occur somewhat rarer.

With the present resolution we may not discriminate between strong magnetic fields in a small portion of the resolution element and, *vice versa*, weak fileds with large filling factors. Brightnesses, velocities, equivalent widths, etc. may have contributions from both magnetic and non-magnetic atmospheric structures, and we don't know the relative filling factors. We measure magnetic fluxes or spatially averaged flux densities. However, from the ubiquitous appearance of the weak IN fluxes, apart from the small tendency of being located in intergranular areas, we may argue that the weak IN elements are not strong enough to withhold the granular flow and that they are just being expelled from the granules. This yields an estimate of the upper limit of the flux density of

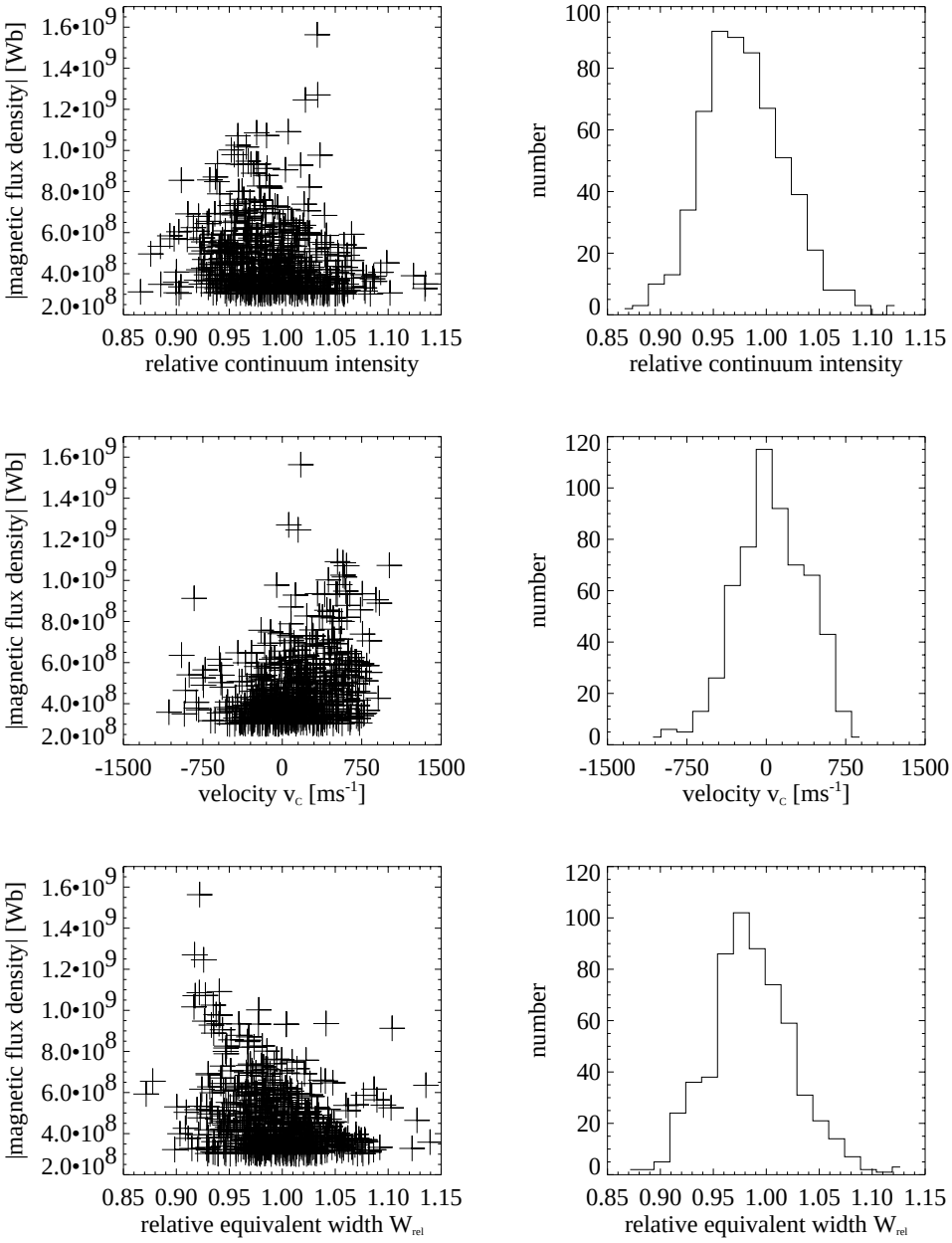

Fig. 4. Left: Scatter plots of $|\Phi|$ *vs* $I_{\rm cont}$, $v_{\rm C}$, and $W_{\rm rel}$. Right: histograms from the analysed points.

$$B^2/(8\pi) \leq \rho v^2\,,$$

i.e. the magnetic pressure is weaker than the flow pressure. With standard values for the density of $\rho \approx 3\,10^{-4}$ kg m^{-3} at the bottom of the photosphere and for the horizontal granular flow velocity of $v_{\rm hor} \leq 2\,10^3$ m s^{-1} we arrive at an upper limit of

$$|B| \leq 5.5\,10^{-2}\ {\rm T}\,.$$

This agrees well with the estimate by Keller et al. (1994) and is within the range of 2–8 10^{-2} T given by Meunier et al. (1998).

5. Conclusion

The micro-image-scanner (MISC) at the GCT and its Stokes-V polarimeter have turned out to be powerful instruments to study magnetic features on the Sun. We achieved high spatial resolution, while sacrificing on high polarimetric accuracy. A lower detection limit for the magnetic flux of 2 10^8 Wb on pixel sizes corresponding to a $0\farcs67\times0\farcs67$ area on the Sun could be obtained by means of a careful data analysis.

There are tendencies that the continuum intensity decreases with increasing flux, that the downward velocity also increases with increasing flux in agreement with the known result that high flux elements are seated in intergranular spaces. The equivalent width and the line center intensity decrease with increasing flux. This latter result is known from the line gaps at locations of magnetic fields (e.g. Stellmacher & Wiehr 1979, Kneer & von Uexküll 1991, Amer & Kneer 1993).

We found well above the detection limit that the weak magnetic flux IN elements do not exhibit a clear, exclusive occurrence in either granules or intergranular spaces. The weaker the

flux, the lower any correlation. Likewise, neither for the direction of the granular flow, nor for the equivalent width, nor for line center intensity, is there found to be a preference of occurrence of weak IN elements. We estimated an upper limit of the magnetic flux density of $|B|_{\mathrm{upper\ limit}} = 55$ mT.

It is certainly important and necessary to confirm, or disprove, this result with substantially higher spatial resolution and/or by other methods such as the multi-line method after Semel (1981). To analyse time sequences and to study the temporal evolution of IN elements at granular and subgranular scales will also be an important further step to elucidate the nature of the IN magnetic fields.

Acknowledgements. The Gregory Coudé Telescope is operated by the Universitäts-Sternwarte Göttingen at the Spanish Observatorio del Teide of the Instituto de Astrofísica de Canarias. This work was supported by the Deutsche Forschungsgemeinschaft through grants KN 152/16-1,-2.

References

Amer M.A., Kneer F., 1993, A&A 273, 30
Donoho D., 1993, Proc. of Symp. in Appl. Math. 47, 173
Durney B.R., De Young D.S., Roxburgh I.W., 1993, Solar Phys. 145, 207
Faurobert-Scholl M., 1996, A&A 268, 765
Keller C.U., Deubner F.-L., Egger U., Fleck B., Povel H.P., 1994, A&A 286, 626
Kneer F., von Uexküll M., 1991, A&A 247, 556
Kneer F., Stolpe F., 1996, Solar Phys. 164, 303
Koschinsky M., Kneer F., 1996, A&AS 119, 171
Krieg J., Wunnenberg M., Kneer F., Koschinsky M., Ritter C., 1999, A&A 343, 983
Lin H., 1995, ApJ 446, 421
Lites B.W., Leka K.D., Skumanich A., Martínez Pillet V., Shimizu T., 1996, ApJ 460, 1019
Livingston W.C., Harvey J., 1975, BAAS 7, 346
Martin S.F., 1988, Solar Phys. 117, 243
Meunier N., Solanki S.K., Livingston W.C., 1998, A&A 331, 771
Neckel H., 1987, FTS-Atlas. Sternwarte Hamburg
Nindos A., Zirin H., 1998, Solar Phys. 179, 253
Petrovay K., Szakály G., 1993, A&A 274, 543
Rees D.E., Semel M.D., 1979, A&A 74, 1
Sánchez Almeida J., Martínez Pillet V., Kneer F., 1995, A&AS 113, 359
Semel M.D., 1967, Ann. Astrophys. 30, 513
Semel M.D., 1981, A&A 97, 75
Smithson R.C., 1975, BAAS 7, 346
Soltau D., 1997, A&A 317, 586
Stellmacher G., Wiehr E., 1979, A&A 77, 263
Stenflo J.O., 1973, Solar Phys. 32, 41
Stenflo J.O., 1982, Solar Phys. 80, 209
Stolpe F., 1998, Ph.D. Thesis, Göttingen University
Stolpe F., Kneer F., 1997, A&A 317, 942
Stolpe F., Kneer F., 1998, A&AS 131, 181
Title A.M., Tarbel T.D., Topka K.P., 1987, ApJ 317, 892
del Toro Iniesta J.C., Semel M.D., Collados M., Sánchez Almeida J., 1990, A&AS 227, 591
Wang H., 1988, Solar Phys. 116, 1
Wang J., Wang H., Tang F., Lee J.W., Zirin H., 1995, Solar Phys. 160, 277
Wang H., Tang F., Zirin H., Wang J., 1996, Solar Phys. 165, 223
Withbroe G.L., Noyes R.W., 1977, ARA&A 15, 363
Zhang J., Lin G., Wang J., Wang H., Zirin H., 1998a, Solar Phys. 178, 245
Zhang J., Wang J., Wang H., Zirin H., 1998b, A&A 335, 341